Numerical Analysis of the ITER TF Conductor Samples in SULTAN With the THELMA Code

Fabrizio Bellina, *Member, IEEE*, Denis Bessette, Marco Breschi, Aldo Di Zenobio, Pier Luigi Ribani, *Member, IEEE*, Laura Savoldi Richard, and Roberto Zanino

***Abstract*—The paper presents the results of a numerical analysis campaign which studies the steady-state behavior and the typical tests (current-sharing temperature and critical current measurements) foreseen for the SULTAN samples of the ITER TF reference conductor, with special emphasis to the current and electric field distribution among and along the sub-cables. In this analysis, the sample geometrical parameters (twist pitch, joint/termination length) and some electrical parameters (joint, termination and inter-bundle resistance) are supposed to range in their design or their measured boundaries, in order to understand their individual effect on the conductor performances and the test conditions.**

***Index Terms*—CICC, ITER, modeling, Nb3Sn, SULTAN samples, superconducting magnets.**

I. Introduction

THE ITER magnets are going to be built starting from next months and their cable in conduit conductor is going to be produced and subjected to the acceptance tests. The production will start with the Nb3Sn TF magnets [1]. To evaluate the validity of the design solutions for their conductor, many samples have been tested so far at the SULTAN facility at PSI in Villigen (CH), under conditions representative of the future operation in the reactor [2]–[7]. These samples differed from each other as regards both the cabling geometrical parameters and the type of strand, and gave quite different performances, in some cases unsatisfactory. To better understand these experimental results and to assess a possible acceptance test procedure to be used for the normal production conductor, a deeper insight in the sample actual test conditions was considered necessary. This paper shows the main results obtained with a simulation campaign carried out with the THELMA code [8], aimed at evaluating the general behavior of the Nb3Sn samples, to make possible a distinction between the cable-specific and the sample general features, and to improve, if possible, the sample arrangement.

Manuscript received August 18, 2008. First published June 05, 2009; current version published July 15, 2009. This work was partly supported by the Italian Ministero dell'Istruzione, dell'Università e della Ricerca as a PRIN Project 2006 and partly by the European Fusion Development Agreement TW7-TMSC-SULMOD. The views and opinions expressed herein do not necessarily reflect those of the European Commission.

F. Bellina is with Università di Udine, Dipartimento di Ingegneria Elettrica, Gestionale e Meccanica, I-33100 Udine, Italy (e-mail: fabrizio.bellina@uniud.it).

D. Bessette is with the ITER IO, Cadarache, 13108 St Paul lez Durance, France (e-mail: Denis.Bessette@iter.org).

M. Breschi and P. L. Ribani are with Università di Bologna, Dipartimento di Ingegneria Elettrica, I-40136 Bologna, Italy (e-mail: marco.breschi@unibo.it; pierluigi.ribani@mail.ing.unibo.it).

A. Di Zenobio is with the ENEA, Centro Ricerche Frascati, I-00044 Frascati, Italy (e-mail: dizenobio@frascati.enea.it).

L. Savoldi Richard and R. Zanino are with Politecnico di Torino, Dipartimento di Energetica, I-10129 Torino, Italy (e-mail: laura.savoldi@polito.it; roberto.zanino@polito.it).

Digital Object Identifier 10.1109/TASC.2009.2018763

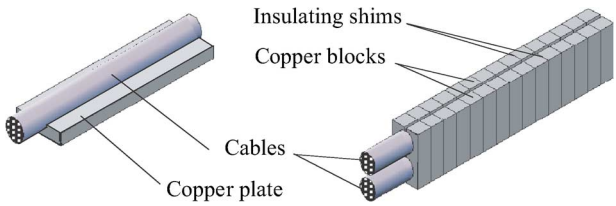

Fig. 1. Sketch of the termination (left) and the joint (right). The steel parts of joint and termination are not represented.

II. Sample Overview

In this analysis, the standard SULTAN samples geometry is considered: two straight segments of ITER full-size jacketed conductor (*legs*), with a total length of about 3400 mm, are connected in series with a resistive joint, located at the bottom of the sample, and are fed by the SULTAN transformer through two resistive terminations. The SULTAN background magnets create a high magnetic field zone (HFZ) in the lower part of the sample, close to the joint. The termination is supposed to be made of a solid steel-copper box, with a seat in the copper plate, in direct contact with the cable. The cable wraps and the sub-cable wraps are supposed to be removed on the cable side facing the copper connection. The lower joint is similar to that described in [9] and is made of two arrays of copper blocks symmetrically placed on both sides of the joint middle plane identified by the two cables. Each block has two seats and is electrically insulated from the adjacent ones by means of insulating shims. A sketch of the termination and the joint is reported in Fig. 1. The reference diagnostic equipment consists of two couples of *crowns* of voltage taps, each made of 6 taps evenly distributed along the jacket azimuthal direction and welded to its surface, located across the HFZ (V3-V9 and Sj1-Sj3, with longitudinal distances $\Delta s = 0.450$, resp. 1.0 m), and two additional crowns with their taps welded at the cable crimping rings (Sc1-Sc3, with $\Delta s = 2.279$ m). The temperature is measured at the inlet and the outlet cooling pipes, located respectively at the lower joint and the upper terminations, and by four sensors on the jacket before / after the HFZ, with $\Delta s = 0.5$ m.

TABLE I
REFERENCE AND BOUNDARY SAMPLE DATA

		Min.	Reference	Max.
Geometric data:				
termination length L_t	(mm)	345	345	420
cable petal twist pitch L_p	(mm)	380	420	460
Resistances:				
termination R_{term}	(nΩ)	0.25	1	3
joint R_{joi}	(nΩ)	0.5	2	4
inter-petal (adjacent) R_{ip}^{ne}	($\mu\Omega$m)	20	200	2000
Conductance:				
cable-jacket σ_{cj}	(kS/m)	5	50	500

III. ANALYSIS SETTING-UP

A. THELMA Code Run Modes and Parametric Approach

The THELMA code was used in two modes:

i) considering the electromagnetic (EM) model with a given temperature profile with time and location,
ii) considering the complete coupled EM and thermal-hydraulic (TH) models.

The first mode saves CPU time and was used for all the runs where the temperature was not a critical model variable (e.g. for the determination of the joint resistance), the second mode was necessary to accurately simulate the superconductor transition due to the helium heating. To carry out the analysis, a parametric variation of some of the model characteristic data, like the cable twist pitch, the contact resistances and so on, was considered. For each of these parameters, the reference value and its boundaries were assumed starting from the typical values of the last tested samples. Conversely, for other model characteristic data, a unique reference value was considered as described in detail below. In the different code runs, one parameter in turn was changed, with all the others at their reference value.

B. Cable Model

To describe the *free cable* (i.e. the cable part outside terminations and joint), we used the THELMA distributed parameter non linear model [8], taking the cable data from the new ITER reference design of the cables [10]. Due to the relatively low n index of the Nb3Sn strand, it is expected that a representation of the cable in terms of its 6 subcables *(petals)* be sufficient. The power law expressing the $E(J)$ in the superconductor makes use of the Summers scaling law for the critical current density $J_c(B,T,\varepsilon)$ [11], assuming $n = 7$, $\varepsilon = -0.5\%$ and $RRR = 120$. In the cable, the inter-petal and the petal-jacket current transfer are influenced by the corresponding conductance per unit of length σ_{ip} and σ_{cj}. It can be shown that, in the six petal model, σ_{ip} can be directly obtained from the inter-petal measured resistance per unit of length R_{ip}^{ne}: $\sigma_{ip} \approx 5/(6R_{ip}^{ne})$. In the model, R_{ip}^{ne} and σ_{cj} are considered independent parameters ranging within the boundaries reported in Table I. The values of R_{ip}^{ne} were taken from the experimental results for the NbTi Cr-coated strands reported in [12]. The different type of superconductor was considered not critical, being the microscopic contact resistance phenomena influenced by the outermost layers of the strands, in both cases made of the same coating.

C. Joint and Terminations Model

No resistive transition is supposed to occur in the superconductor inside the joint and the terminations, therefore a linear lumped network was used for this sample part [13]. No copper magnetoresistance is taken into account. Both the joint and the terminations have been modeled in two ways, characterized by a different level of detail. In the first way, the joint/termination corresponds to a 3D linear lumped network in which the contact resistances between the petals and the termination/joint copper parts are computed starting from the component geometry. Both the petals and the copper can be modeled as sets of resistive/inductive network components, in order to study also EM diffusion phenomena. This model is directly interfaced with the free cable model so that, in this case, the EM boundary conditions are set directly for the two terminations. In the second way of representation, the joint and the terminations are simply described each as 0D linear resistive network N-pole, without any inductive property, connected to the free cable petals ends. Each of these network components is characterized by its resistance matrix $\mathbf{R}$, such that the cable model boundary conditions can be expressed as $\mathbf{U} = \mathbf{RI}$, being $\mathbf{U}$ the array of the voltages between each petal end and the reference and $\mathbf{I}$ the array of the petal end currents. In steady state, this representation of the joint/termination is exact, moreover, it showed to be applicable also in transient regime with negligible errors, at the reference current ramp-rate values.

D. Thermal-Hydraulic Model

The TH model included in the most recent version of the THELMA code is derived from [14]. It solves 1D compressible (Euler) flow along an arbitrary number of *channels* coupled to 1D heat conduction along an arbitrary number of cable elements (here corresponding to the petals) and a single jacket. The coupling with the EM modules inside THELMA is achieved by exchanging temperature and heating power distributions.

IV. ANALYSIS RESULTS

A. Steady-State Analysis

A preliminary set of steady-state analyses was carried out with the individual 3D detailed models of the joint and the terminations, to fit the sample reference and boundary resistance values of R_{term} and R_{joi} reported in Table I by trimming the distributed contact resistances in the termination and the joint, R_{term}^{d} and R_{joi}^{d}. In these models, the termination/joint was represented together with the relevant part of cable, whose petals were all short-circuited and fed with an impressed steady voltage, applied between the cable and the resistive saddle (in the case of the terminations) or between the two cables (in the case of the joint). The distributed additional contact resistance $R_{pt_a}^{d}$ representing the effect of the petal wrapping was then determined as $R_{pt_a}^{d} = 1/(2\sigma_{ip})$.

Two 3D models of the complete sample (two legs) and half sample (one leg) with the detailed representation of terminations and joint (half joint, in the latter case) have then been used to compute the steady-state distribution of the currents and voltages and to build the resistance matrices for the simplified 0D

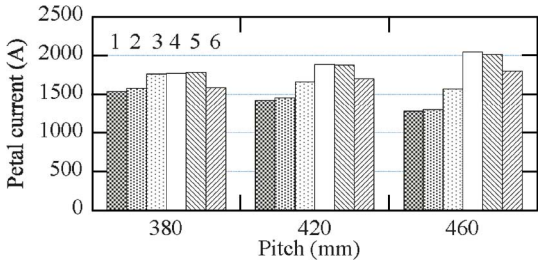

Fig. 2. Steady-state 3D model of one leg. Petal currents for different twist pitches L_p with a transport current of 10 kA. Reference termination length L_t.

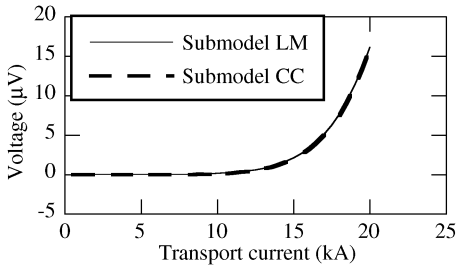

Fig. 3. Critical current simulation. Average voltage along the petals of the left leg computed across the HFZ.

representation of joint and terminations. In this way, the geometrical coherence between the angular position of the petals in the terminations and the joint was guaranteed and the effect of the cable twist pitch was taken into account. In all these analyses, no petal resistive transition was considered, so that the cable petals could be modeled as ideal short circuits. These computations have shown that, for all the range of inter-petal resistance R_{ip}^{ne}, the current is almost uniform along each petal in the free cable, which means that the current transfer between adjacent petals is almost negligible in the superconductive steady-state. This may not hold for the smaller bundles, not represented in this model. The current is not uniformly distributed among the petals, due to the uneven contact between the petals and the copper plate of the terminations, which is shorter than the cable twist pitch. With the reference termination length, the current unbalance is almost independent on the termination/joint resistances, while it remarkably increases with the cable twist pitch, as visible in Fig. 2, which was obtained with the detailed model of half sample. Additional simulations showed that the current becomes almost uniformly distributed among the petals when the termination is as long as the twist pitch. The results of the computation of the resistive matrices of terminations and joint have shown that, as regards the two terminations, the mutual resistances R_{ij} are far lower than the self resistances R_{ii} (3 orders of magnitude) for all the range of contact resistances, therefore a *star of resistors* can be a suitable model to represent the terminations in steady-state. Instead, in the case of the lower joint, due to the presence of the transverse insulating shims, the mutual resistances are quite comparable with the self resistances. In this case, the joint representation in terms of an equivalent resistive N-pole is compulsory.

B. Transient Regime Analysis

1) Response to the Ramp of Current (I_c Test Simulation): The 3D model of the complete sample was studied also in transient regime, with the aim at evaluating the effect of the joint and termination on the overall sample behavior. Among the cases considered, we report here the response to a ramp of current of 1 kA/s representing a critical current (I_c) test. In these analyses, the cable inside terminations/joint is modeled alternatively with lumped coupled inductive components *(submodel LM)* or simple short-circuits *(submodel CC)* [13]. The second submodel would be preferable to the first one, being characterized by a much lower number of inductive parameters and state variables, therefore needing less CPU time for its solution. Fig. 3

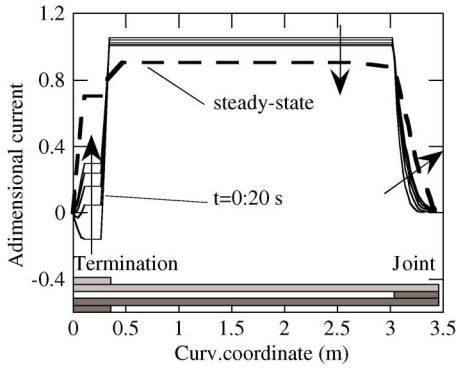

Fig. 4. Critical current simulation, submodel LM. Current along petal #1 of the left leg for different time values. The arrows show the change of the current waveforms with time. A sketch of the sample is reported at the bottom of the graph.

reports the average voltage along the petals of the left leg, taken across the HFZ $(\Delta s = 0.450\,\mathrm{m})$ for the two submodels at a constant temperature of 9 K. Such a high temperature has been set in order to get an early cable transition, to save computation time. The graph shows that almost coincident voltage waveforms (and therefore the same working conditions for the free cable superconductor) were obtained from the two submodels. Thus, the submodel CC is suitable to analyse the I_c at the reference current ramp rate, with the cable modeled in terms of its petals. This may not be applicable for more detailed cable representations or higher ramp rates. Actually, large current diffusion phenomena take place inside the joint and the terminations, even if their effects on the I_c are almost negligible. The petal current distribution is expressed here in terms of *adimensional currents,* defined as: $i_k^a(s,t) = i_k(s,t)/i_k^{id}(t)$, where $i_k(s,t)$ is the current in the k-th petal at the curvilinear coordinate s and time t, and $i_k^{id}(t)$ is the corresponding ideal value, uniform among and along the petals. Fig. 4 compares the adimensional current along petal #1 for different time values. The currents in the other petals have a similar behavior. To prevent an early transition, in this case the cable temperature was suitably lowered, so that the sample had always a linear behavior. As it can be seen, in the joint/terminations zones, i_k^a can be even negative while, in the free cable, the change of i_k^a is smaller, but characterized by very long time constants (hundreds of seconds) due to the low joint/termination resistances and to the overall sample inductance.

2) Analysis of a T_{cs} Test: The coupled EM+TH models were used to simulate a current sharing (T_{cs}) test, considering one leg only, the other being represented by a single solid conductor,

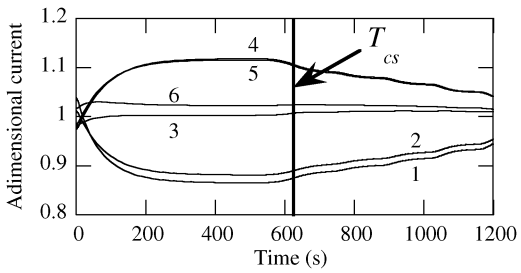

Fig. 5. Simulation of a T_{cs} test. Computed adimensional current evolution with time.

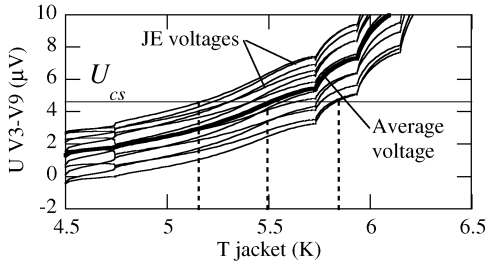

Fig. 6. Simulation of a T_{cs} test. Jacket voltage across the HFZ at the JE azimuthal locations as a function of the jacket temperature downstream.

to account for its inductive effects. The helium initial temperature is $T_0 = 4.5$ K, followed by a ramp of current up to the plateau value $I = 68$ kA @ 10 kA/s, with an external field $B = 10.78$ T and a plateau of 500 s before starting the cable heating. All the model parameters have their reference value. To achieve a faster computation, the terminations and the joint are represented by their equivalent resistance matrices. Each petal is characterized by its own temperature $T_k(s,t)$ and six cooling channels are individually modeled (the central channel is supposed to be plugged). These analyses make use also of the jacket EM model, recently developed to compute the voltage signals taken on the jacket surface [15]. The jacket is described by a resistive-inductive distributed parameter model which considers currents both in the jacket longitudinal and azimuthal directions, due to the resistive contact with the petals and to their inductive effects, non negligible during the transient phases. In these analyses, the jacket was discretized into 12 *jacket elements* (JE) along the cable azimuthal directions, so that the voltage between taps could be computed directly as voltage along some JE. The results of the simulation were evaluated in terms of petal current distribution and T_{cs}, defined here, consistently with the experiment, as the jacket temperature downstream of the HFZ when the voltage U between V3 and V9 crowns corresponds to the critical field $E = 10^{-5}$ V/m($U_{cs} = 4.5\ \mu$ V). For each JE azimuthal position, U is computed along the jacket longitudinal direction. During heating, the current distribution evolves towards a uniform distribution, as reported in Fig. 5. The computations showed also that the petal current remains almost uniform along the cable, i.e. the current redistribution takes place in the joint/termination only. Fig. 6 shows the computed jacket voltage-temperature characteristics at the JE azimuthal locations and outlines the U_{cs} value. From this figure one can see that, when U is given by a *single couple of taps*, the T_{cs} would stay outside ± 0.25 K from the value determined on the basis of the average U. This means that the non-uniformity of the voltage signals along the jacket azimuthal direction has a noticeable effect on the determined T_{cs}. The analyses showed also that, in this case, the average $U(T)$ curve obtained from the values computed on the jacket is very close to the average curve computed along the petals, while a spread of ≈ 1 K is found if the T_{cs} were determined considering the voltage of each petal individually and assuming a uniform current distribution. This is due to the non-uniform current distribution among the petals which, in addition, are subjected to a different magnetic field strength in the HFZ.

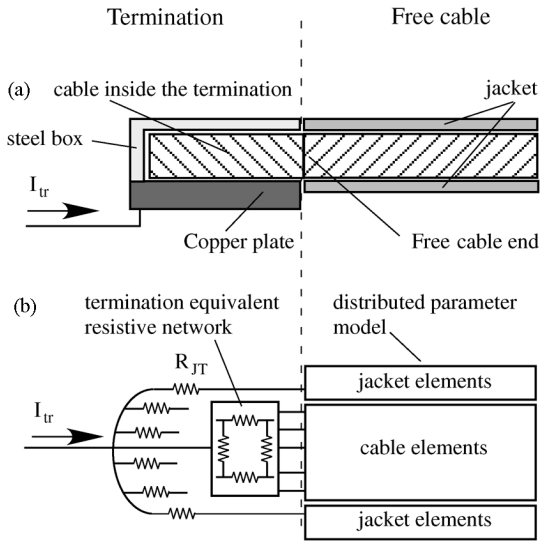

Fig. 7. (a) Topology of the cable + jacket - termination interface. (b) Equivalent networks to model the boundary conditions.

3) Effect of Joint/Terminations on the Voltage Measurements: Both the terminations and the joint are electrically connected to the jacket through a stainless steel structure, and this connection may affect the voltage distribution at the jacket taps. For this reason, we analysed the same T_{cs} test including also a very simple electrical model of the steel box surrounding the termination/joint, consisting of a star of equal resistors R_{JT} connected between the end of each JE and a suitable node of the lumped network of the termination/joint, here represented by with the submodel CC (Fig. 7) [16]. Fig. 8 shows the voltage signals between the crowns Sc1-Sc3, Sj1-Sj3 and V3-V9 in correspondence of $R_{JT} = 2 \cdot 10^{-3}\ \Omega$. This resistance value was obtained from a best-fit of the computed with the measured voltages waveforms for a set of samples recently tested. It can be seen that a bias voltage is present between the voltage taps well before any resistive transition. This voltage is not due to inductive effects, nor to a cable longitudinal resistance, but only to the currents in the jacket, due to its contact with the petals and with the steel box surrounding the joint and termination. Due to the relatively high resistivity of the jacket and joint/termination boxes, these currents are small, compared with the petal currents, nevertheless their effect on the voltage distribution is quite comparable with the effect of the free cable end of the joint/terminations.

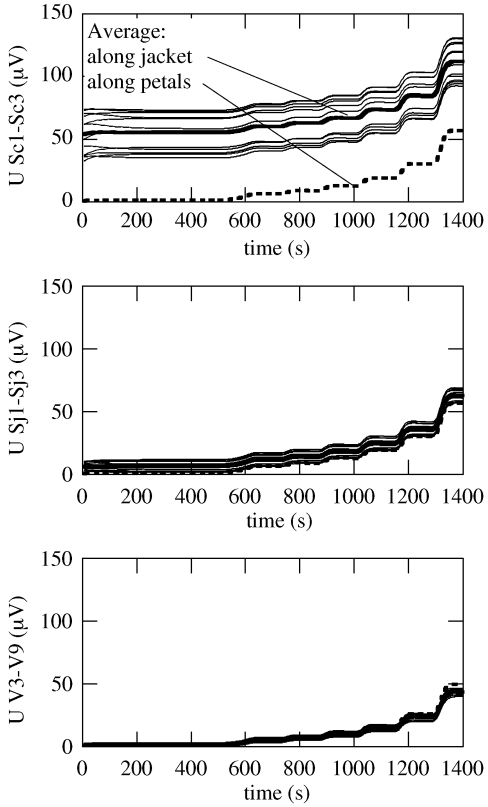

Fig. 8. Simulation of a T_{cs} test. Voltages between cable sections Sc1-Sc3, Sj1-Sj3, V3-V9.

The longer the distance between the voltage taps and the termination/joints, the lower is the bias voltage. On the other hand, this effect depends also on the value of the conductance σ_{cj} between cable and jacket: the higher the conductance, the lower is the bias. According to this simple model, and with the parametric values assumed, at the high field region voltage taps V3-V9, the bias voltage is almost negligible.

V. Conclusion

A set of remarks and recommendations can be made on the basis of the analyses carried out with the THELMA code. The termination length should be at least as long as the longest foreseen petal twist pitch, which should be known exactly from measurements, since the difference between the nominal and the actual value may change dramatically the experimental results. The actual value of the jacket-petal resistance should be known, as it strongly affects the voltage signals scattering which, for this reason, cannot be considered in itself as an index of the sample quality. The accuracy of the joint and termination resistance measurement should be carefully assessed, taking into account the influence of the joint /termination on the jacket voltage, since this resistance directly affects the computation of the joule losses, as well as the spectrum of electromagnetic time constants. The analyses have also shown that the T_{cs} assessment based on a single voltage measurement can be subjected to non negligible errors, depending on the taps position along the cable. In our simulations, these errors are greatly reduced when the average voltage between the couple of crowns is used.

References

[1] N. Mitchell *et al.*, "The ITER magnet system," *IEEE Trans. Appl. Supercond.*, vol. 18, no. 2, pp. 435–440, June 2008.

[2] P. Bruzzone *et al.*, "Upgrade of operating range for SULTAN test facility," *IEEE Trans. Appl. Supercond.*, vol. 12, no. 1, pp. 520–523, March 2002.

[3] P. Bruzzone *et al.*, "Results of a new generation of ITER TF conductor samples in SULTAN," *IEEE Trans. Appl. Supercond.*, vol. 18, no. 2, pp. 459–462, June 2008.

[4] P. Bruzzone *et al.*, "Test Results of Two European ITER TF Conductor Samples in SULTAN," *IEEE Trans. Appl. Supercond.*, vol. 18, no. 2, pp. 1088–1091, June 2008.

[5] Y. Takahashi *et al.*, "Performance of Japanese $\mathrm{Nb_3Sn}$ conductors for ITER toroidal field coils," *IEEE Trans. Appl. Supercond.*, vol. 18, no. 2, pp. 471–474, June 2008.

[6] H. C. Kim, D. K. Oh, S. H. Park, K. Kim, and P. Bruzzone, "Development and sultan test result of ITER conductor samples of Korea," *IEEE Trans. Appl. Supercond.*, vol. 18, no. 2, pp. 1084–1087, June 2008.

[7] D. Bessette and N. Mitchell, "Review of the results of the ITER toroidal field conductor R&D and qualification," *IEEE Trans. Appl. Supercond.*, vol. 18, no. 2, pp. 1109–1113, June 2008.

[8] M. Ciotti, A. Nijhuis, P. L. Ribani, L. S. Richard, and R. Zanino, "THELMA code electromagnetic model of ITER superconducting cable and application to the ENEA stability experiment," *Supercond. Sci. Technol.*, vol. 19, pp. 987–997, 2006.

[9] P. Bruzzone, "Manufacture and performance results of an improved joint for the ITER conductor," *Adv. Cryog. Eng.*, vol. 45, pp. 737–744, 2000.

[10] D. Bessette, "Change of the Reference TF Conductor (Performance Qualification Samples)," presented at the ITER Conductor Meeting, July 2–3, 2007, PSI, Villigen, unpublished.

[11] L. T. Summers, M. W. Guinan, J. R. Miller, and P. A. Hahn, "A Model for The Prediction of Nb3sn Critical Current as a Function of Field, Temperature, Strain, and Radiation Damage," *IEEE Trans. Magn.*, vol. 27, no. 2, pp. 2041–2044, March 1991.

[12] A. Nijhuis, Y. Ilyin, W. Abbas, B. ten Haken, and H. H. J. ten Kate, "Change of interstrand contact resistance and coupling loss in various prototype ITER NbTi conductors with transverse loading in the Twente Cryogenic Cable Press up to 40,000 cycles," *Cryogenics*, vol. 44, pp. 319–339, 2004.

[13] F. Bellina, "The THELMA electromagnetic model of the poloidal field conductor insert (PFCI) joint," *IEEE Trans. Appl. Supercond.*, vol. 17, no. 2, pp. 2381–2385, June 2007.

[14] L. Savoldi Richard, M. Bagnasco, and R. Zanino, "Multi-solid Multi-channel Mithrandir (M3) code for thermal-hydraulic modelling of ITER Cable-in-Conduit Superconductor," *Fus. Eng. Des.*, vol. 82, pp. 1607–1613, 2007.

[15] M. Breschi and P. L. Ribani, "Electromagnetic Modeling of the Jacket in Cable-in-Conduit Conductors," *IEEE Trans. Appl. Supercond.*, vol. 18, no. 1, pp. 18–28, March 2008.

[16] M. Breschi, L. Ribani, and F. Bellina, Electromagnetic Analysis of the Voltage-Temperature Characteristics of ITER TF Conductor Samples this Conference.